Plant, Cell & Environment

WILEY

Plant, Cell & Environment

ORIGINAL ARTICLE OPEN ACCESS

Allometric Relationships of Branch Water-Storage Capacity and Capacitance in Four European Trees Species

Sonia Hernando[1,2] | Oliver J. Binks[2] | Jordi Martínez-Vilalta[1,2] | Nicolas K. Martin-StPaul[3] | Sylvain Delzon[4] | Maurizio Mencuccini[2,5]

[1]Department of Animal Biology, Plant Biology and Ecology, Universitat Autònoma de Barcelona, Cerdanyola del Vallès, Barcelona (Catalonia), Spain | [2]CREAF, Cerdanyola del Vallès, Barcelona (Catalonia), Spain | [3]URFM, INRAe, Avignon, Provence-Alpes-Côte d'Azur, France | [4]UMR BIOGECO, INRAe, University of Bordeaux, Pessac, Nouvelle-Aquitaine, France | [5]ICREA, Barcelona, Barcelona (Catalonia), Spain

Correspondence: Sonia Hernando (Sonia.Hernando@autonoma.cat)

Received: 3 October 2024 | **Revised:** 8 January 2025 | **Accepted:** 10 January 2025

Funding: The study was supported by the European Social Fund, MCIN/AEI/10.13039/501100011033 (grants CEX2018-000828-S and PRE2021-098897), Agència de Gestió d'Ajuts Universitaris i de Recerca de Catalunya (grant 2021 SGR 00849), Institució Catalana de Recerca i Estudis Avançats, 'la Caixa' Foundation, and Horizon 2020 Framework Programme (grant 862221).

Keywords: allometry | capacitance | functional traits | tissue proportions | water release curve | water storage capacity

ABSTRACT

Water storage capacity and capacitance in trees regulate hydration levels, providing water reserves during drought. However, the effects of varying traits, tissue fractions and of different water pools on the allometry of branch-/sample-level properties have not been systematically investigated. We analyse the relationships between branch size and branch capacity and capacitance with respect to wood density, xylem vulnerability to embolism, and tissue fractions. The analysis was performed using data from four tree species sampled from 12 to 15 sites across Europe. We show that of the three phases of the water release curve, the second phase (dominated by elasticity) was significantly influenced by leaf and bark proportions, the sapwood/heartwood ratio and xylem vulnerability to embolism for capacity and/or capacitance. However, the first (dominated by capillarity) and the third phase (characterised by embolism) were not influenced by the morpho-physiological properties measured. Our results indicate that branch capacity and capacitance are allometrically related (slope < 1) to branch dry mass, leaf area and total water content, indicating that normalising by these size measures does not completely remove size-dependency. We conclude that the only means of obtaining size-independent water storage traits directly applicable in comparative and modelling studies is by normalising by water quantity per phase.

1 | Introduction

Tissue water storage influences diverse facets of tree development, functioning and adaptation to environmental changes, such as drought stress (Holbrook 1995). Water storage helps to maintain hydraulic continuity from roots to leaves under fluctuating water availability (Brodribb and Holbrook 2003; Meinzer et al. 2003; Scholz et al. 2007; Meinzer et al. 2008). Stored water can maintain cell turgor and prevent stomatal closure, particularly in dry conditions when water uptake from soil is limited (Holbrook 1995; Brodribb and Holbrook 2003). After stomatal closure, total water storage capacity and hydraulic capacitance influence the time to desiccation during extreme drought (Blackman et al. 2016), thereby delaying drought-induced mortality (Martin-StPaul, Delzon, and Cochard 2017).

Water is stored throughout all tissues in trees, and principally the xylem (Tyree and Zimmerman 2013) where cavitation in conduits and fibres can release significant quantities of water

(Tyree and Yang 1990). In sapwood, water is also stored and released from intercellular capillary spaces (Holbrook 1995), whereas the importance of sapwood living cells for capacitance is still debated (Pratt et al. 2021; Jupa et al. 2016; Ziemińska et al. 2020). Heartwood water storage may also play a role in buffering plant water status, although the extent of this effect is still unclear (Hu et al. 2018). Water storage in leaves (Tyree and Ewers 1991) and inner bark, for example, the phloem (Pfautsch, Hölttä, and Mencuccini 2015) is dominated by the elastic deformation of cells, facilitating the movement of water without large turgor changes. Given that water storage properties are typically measured at organ level, and that tissue fractions are highly variable both within- and among-plants, a key question remains on how to scale them to obtain meaningful traits for the whole plant.

Tree water storage is quantified via water storage capacity and capacitance (Scholz et al. 2011). Capacity represents the total volume of water that is contained or can be extracted from the tissue, and capacitance is the (reversible or irreversible) change in storage per unit change in water potential (Hartzell, Bartlett, and Porporato 2017). Tree water storage is characterised using the relationship between water potential and water loss, known as the water release curve/pressure-volume curve. Understanding the extent to which water release curves differ across tissues, organs and species can contribute to a better knowledge of the maintenance of water balance (Jupa et al. 2016; Scholz et al. 2007). Tyree and Yang (1990) proposed a conceptual model to interpret water release curves in leafless branches (referred to as TY1990), where the curve consists of three phases, each characterised by distinct water potential ranges. Phase I includes the capillary release of water from xylem conduits and intercellular spaces, occurring at high water content and water potentials, typically ranging from 0 to −0.5 MPa. Phase II is dominated by the elastic release of water from living tissues, potentially overlapping with capillary release at water potentials ranging from −0.5 to −1.5 MPa. Phase III may be associated with the release of water during embolism when air enters xylem conduits, occurring at low water potentials (Hölttä et al 2009). This final phase is a critical point whereby plants undergo significant water stress, and continued reductions in water potential may result in irreversible damage to the xylem water transport system (Mantova et al. 2022). In the case of *Pinus, Populus* and *Fagus*, the three genera examined in this work, the transition from the initial phases to the cavitation phase in the water release curves of stem segments in a cavitron occurs before the P50 point in the vulnerability curve (Pivovaroff et al. 2016).

Despite its importance for our understanding of water release by woody structures, the TY1990 model has seldom been tested. Direct tests are complicated by the difficulty of completely separating the processes controlling the three proposed phases.

We propose here instead an indirect test of the TY1990 model based on allometric theory, i.e., by examining how the different processes linked to the three phases change as branches increase in size. In the context of allometric analysis of water storage, isometry assumes a linear relationship between water storage properties and branch size, while allometry recognises that these relationships may be curvilinear. In a linear relationship with zero intercept, the ratio of water storage to size gives a size-normalised (i.e., size-independent) value. However, this is not the case if the relationship is curvilinear. In this case, the ratio of water storage to size will remain size dependent. Allometry examines whether, as branches vary in size, changes in structural organisation, tissue fractions, and physiological functions result in non-linear (i.e., allometric) relationships (Niklas 2004). By way of example, larger branches have a greater volume. Consequently, larger branches may have proportionally higher water storage compared to smaller branches. However, if tissue fractions, such as the heartwood fraction, vary with the dimensions of the branch, then water storage capacity and capacitance will not vary linearly with branch size, but with a slope changing in proportion to the volumetric fraction of each tissue (Pérez Cordero and Kanninen 2003; Aparecido et al. 2016).

We refer to un-normalised capacity and capacitance as extensive and to the size-normalised versions as intensive properties (where extensive properties scale with size, while intensive properties are independent of size) (Mc Naught and Wilkinson 2014, IUPAC Gold Book). Branch-level capacity and capacitance are commonly normalised either using branch dry mass (e.g., Bryant et al. 2021; Beckett et al. 2024), total saturated mass in RWC units (e.g., Domec and Gartner 2001; Li et al. 2018), or leaf area (e.g., Ruffault et al. 2022). With isometric relationships, these standardisations eliminate size-dependency, i.e., the exponent of the intensive properties against size is zero. However, these normalisations may be misleading with allometric relationships, because when the exponent of extensive properties against size is different from 1 or the y intercept is different from 0, the normalised property will remain size-dependent and therefore not truly intensive. For these reasons, exploring the allometric relationships of extensive and size-normalised (presumably intensive) water storage properties against mass is a key objective of this study.

The main aim of this work is to explore the allometry of capacity and capacitance in the three distinct phases of a branch water release curve. Because multiple authors normalise capacity and capacitance by branch size (e.g., Gleason et al. 2014, Wolfe and Kursar 2015; Bryant et al. 2021), our first null hypothesis is that extensive branch water storage properties have an isometric relationship with size, that is, with an exponent of the log–log relationship of 1.00. Conversely, if the relationship is allometric, the slope against mass should be different from 1.00. Specifically, the slope of the log–log relationship will be lower than 1.00 if the sizes of the water pools that are released during the three phases vary less than proportionally with size. Consequently, if the relationship is allometric, normalising water storage by either branch mass, leaf area or total water content will not eliminate the size-dependency of these properties.

Second, if allometric relationships are explained by a trait related to the different processes controlling the three phases of the TY1990 model, then incorporating that trait in the regression should increase the allometric exponent to a value closer to 1.00. We tested whether allometric relationships of water storage properties are affected by branch wood density (WD), xylem vulnerability to embolism, and changes in tissue proportions

between sapwood and heartwood and between branch leaf, bark and wood mass. Our second set of predictions are that (a) WD affects the allometry of all three phases of the water release curve, albeit not equally. We also expect (b) vulnerability to embolism (as quantified by xylem P50, cf., Table 1 for definitions) and the heartwood ratio to affect the allometry only in Phase III, which includes the discharge of embolism water and residual water from the heartwood. Finally, we predict (c) that leaf and bark proportions affect the allometry of Phase II (elastic water release), while wood proportion affects Phase I (capillary water release) and Phase III.

Our third and final prediction is that, if the hypotheses embedded in TY1990 are correct, the three phases of the model refer to functionally distinct pools of water. In other words, that these pools are released because of different processes. Therefore, employing the water content of each phase (instead of branch dry mass, leaf area or total water content) as basis for size-normalisation should result in size-independent properties (size-normalised exponent =0). However, if the phases refer to a single functional pool, this normalisation should still result in size-dependency (size-normalised exponent ≠0).

2 | Materials and Methods

2.1 | Study Sites, Species and Sampling Design

Four species were sampled across a large portion of their natural range in Europe, with each species being measured at 12–15 sites (see map, Supporting Information: Figure S1). The sites were selected within protected areas (Gene Conservations Units, part of EUFORGEN, de Vries et al. 2015). Black poplar (*Populus nigra* L.) and maritime pine (*Pinus pinaster* Ait.) were sampled in 2021, European beech (*Fagus sylvatica* L.) and Scots pine (*Pinus sylvestris* L.) in 2022. The two angiosperms were sampled during spring/early summer to capture branches under full foliation but before the onset of summer drought. The evergreen conifers were sampled instead during autumn. At each site, 10 individual trees were sampled in parallel transects separated by at least 30 m of distance from one another. Two to three branches with a length of about 1.5–2.0 m were cut from the top of each tree on which branch-level capacitance, xylem vulnerability to embolism, and WD were determined. Following sampling, branches were recut under water to obtain subsamples for capacitance with different sizes for each species: *Populus nigra* and *Pinus pinaster* (40–50 cm), *Pinus sylvestris* (40–60 cm) and *F. sylvatica* (70–80 cm). Branch length corresponds to the distance from the branch tip to the base. Even if branch length was standardised within species, there was substantial variation in total branch biomass, largely due to variations in branching structure and location of the sample. Different lengths were chosen for different species to obtain always more than 20 leaves, twigs or brachyblasts per branch for water potential measurements. Branches were temporarily stored in the field in the shade inside a double black plastic bag with wet paper towels and then shipped to the laboratory, where they were stored in a cold chamber (4°C–10°C). For hydraulic conductivity and vulnerability to embolism, different branch subsamples were obtained from the same branches by cutting 50-cm-long straight segments. These branches were also stored inside sealed wet bags, shipped to the laboratory and kept in a refrigerated room at 6°C before their measurements. Measurements of branch water release curves and vulnerability to embolism were done less than a week from collection. Total sample size was 545 branches across the four species.

2.2 | Branch Dehydration Experiment

Our protocol broadly followed Gleason et al. (2014). In the laboratory, branch bases were submerged and the bottom 5 cm of the branch re-cut under water. Branches were then left in a cold chamber at 5°C to saturate overnight inside a black plastic bag. The following morning, branches were equilibrated at air temperature for 15 min inside a black plastic bag with a small ball of wet paper towel inside. One or two leaves (*Populus nigra*), small twigs (*F. sylvatica* and *Pinus sylvestris*) or brachyblasts (*Pinus pinaster*) were cut from the branch and their water potential (Ψ_P) measured in a PMS 1505D pressure chamber (PMS Instruments, Albany, OR, USA). The branch was then weighed and left to desiccate in a temperature-controlled room using a fan to stir the air. For the two pine species, an oven equipped with a water-filled tray and with temperature set at 30°C was employed in some cases to speed up the desiccation process towards the end of the curve. In both cases, temperatures and humidity were monitored continuously. Using cycles with variable dehydration times (depending on the species), the branch was put back inside the plastic bags for 15–20 min to equilibrate, to allow the leaf to approximate the water potential of the stem, and each step was then repeated for at least 11 more times. Our curves therefore were carried out under quasi-equilibrium conditions (as in standard PV curves), something that would be impossible to do under in vivo conditions.

Because of logistical limitations due to the large number of samples to process, the experiment generally ended at a pressure balance of around 3 MPa. For all four species, this value went beyond the end of Phase II of the stem dehydration, while the third phase involving embolism was covered to a variable extent.

2.3 | Capacity and Capacitance

We analysed water release by splitting the curve into three parts, using cut-off points (see Figure 1). The lowest (most negative) limit for Phase I (capillarity) was taken as the inflection point of the curve of moisture release against water potential (Ψ), using a segmented function in R (Muggeo and Muggeo 2017). The inflection point differed for each species (*Populus nigra* $\Psi = -0.272$ MPa, *Pinus sylvestris* $\Psi = -0.230$ MPa, *Pinus pinaster* $\Psi = -0.178$ MPa and *Fagus sylvatica* $\Psi = -0.220$ MPa). Values comprised between these species-specific inflection points and the branch-specific P12 (pressure inducing 12% loss of conductivity), were employed to quantify the elastic phase (Phase II). Finally, values below P12 were used to estimate the third phase, when cavitation becomes prevalent. Note that this study included leaves in branches, while TY1990 did not. Consequently, the pool of water coming from leaves might influence significantly the elastic phase, and as a result the Ψ thresholds limiting this phase may not correspond exactly with those of TY1990. Specifically in

TABLE 1 | A primer of terms and symbols used in this study.

Symbol	Meaning	Units
Ψ	Water potential	MPa
M_{branch}	Dry mass of the branch	g
S_{branch}	Saturated mass of the branch	g
% wood	Percentage of the dry mass of the wood with respect to the sum of bark, leaves and wood dry masses	%
% bark	Percentage of dry mass of the bark with respect to the sum of bark, leaves and wood dry masses	%
% leaves	Percentage of dry mass of the leaves with respect to the sum of bark, leaves and wood dry masses.	%
prop_heartwood	Heartwood ratio. Proportion of non-active xylem cross-sectional area with respect to stem cross-sectional xylem area without bark.	proportion
WD	Wood Density. Calculated as: $\frac{\text{Dry mass wood}}{\text{Fresh wood volume}}$	g cm^{-3}
P50	Water potential at 50% loss of hydraulic conductivity. Obtained from vulnerability curves (Delzon et al. 2010)	MPa
P12	Water potential at 12% loss of hydraulic conductivity. Obtained from vulnerability curves (Delzon et al. 2010)	MPa
$W_{I\ max}$	First and maximum branch mass measured in the phase I of the water release curve	g
$W_{I\ min}$	Last and minimum branch mass measured in the phase I of the water release curve	g
$W_{II\ max}$	First and maximum branch mass measured in phase II of the water release curve	g
$W_{II\ min}$	Last and minimum branch mass measured in the phase II of the water release curve	g
$W_{III\ max}$	First and maximum branch mass measured in the phase III of the water release curve	g
$W_{III\ min}$	Last and minimum branch mass estimated in the phase III of the water release curve	g
P_{II}	Last water potential measured in the phase II of the water release curve	MPa
P_{III}	First water potential measured in the phase III of the water release curve	MPa
W_{P12}	Branch mass estimated at P12. Calculated as: $W_{P12} = W_{II\ min} + \frac{(W_{III\ max} - W_{II\ min})}{(P_{III} - P_{II})} * (P12 - P_{II})$	g
W_{P99}	Branch mass estimated at P99, assuming 25,2% of moisture content	g
P99	Water potential at 99% loss of hydraulic conductivity. Obtained from vulnerability curves (Delzon et al. 2010)	MPa
WS	Branch capacity, calculated as: Phase I: $W_{I\ max} - W_{I\ min}$; Phase II: $W_{II\ max} - W_{II\ min}$; Phase III: $W_{P12} - W_{P99}$	g H_2O
C_e	Extensive branch capacitance, calculated as the slope of the linear relationship between weight of water loss and Ψ Phase I and II: $-\frac{\Delta \text{water loss}}{\Delta \Psi}$; Final part: $\frac{WS_{Phase\ III}}{P12 - P99}$	g H_2O MPa^{-1}
c_{DM}	Intensive branch capacitance normalised by dry mass. Calculated as: $\frac{C_e}{M_{branch}}$	g H_2O g^{-1} MPa^{-1}
c_{WC}	Intensive branch capacitance normalised by phase water content. Calculated as: Phase I: $\frac{C_e}{W_{I\ max} - W_{I\ min}}$; Phase II: $\frac{C_e}{W_{II\ max} - W_{II\ min}}$; Phase III: $\frac{C_e}{W_{P12} - W_{III\ min}}$	RWC MPa^{-1}
c_{TWC}	Intensive branch capacitance normalised by total water content. Calculated as: $\frac{C_e}{S_{branch} - M_{branch}}$	RWC MPa^{-1}
c_{LA}	Intensive branch capacitance normalised by leaf area. Calculated as: $\frac{C_e}{\text{Leaf area}}$	$gH_2Ocm^{-2}MPa^{-1}$

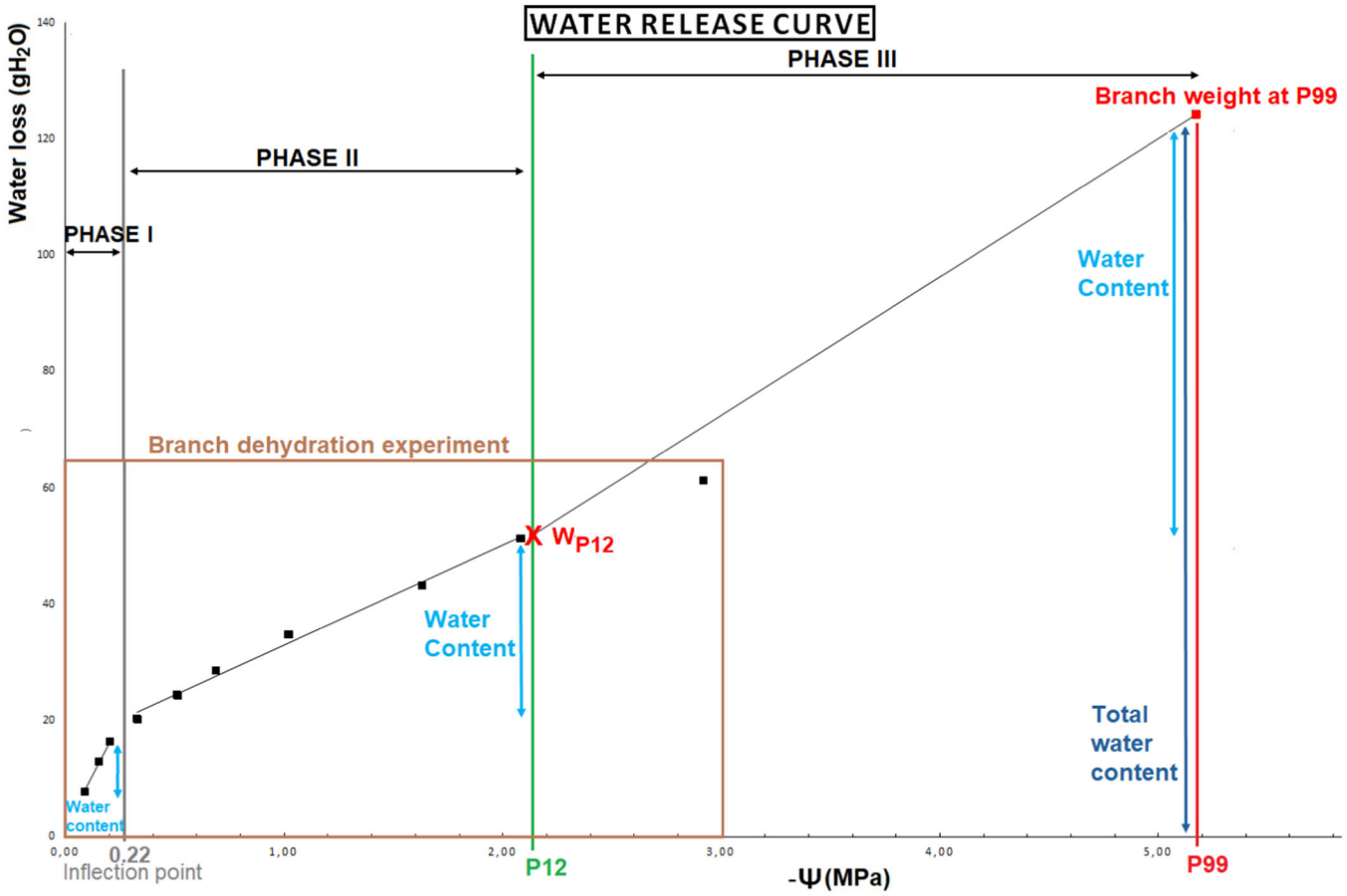

FIGURE 1 | Scheme of the approach used in this study to calculate capacity and capacitance for the three parts of the curve. The figure shows the relationship between water loss (%) and water potential (−Ψ, MPa) obtained from the branch dehydration experiment. The brown square marks the zone where measurements were taken. The curve was split into three parts, based on two cut-off points. The first part (extreme left, dominated by capillarity) includes all points above inflection point (grey line). The second part is between the inflection point (grey line) and P12 (Ψ causing 12% loss of conductivity) of the vulnerability curve (green line) and defines the elasticity phase. The third and final part included all points measured at Ψ < P12 plus one estimated point at P99 when the branch was assumed to have reached 25.2% equilibrium moisture content (point in red) (Engelund et al. 2013 and Ross 2010). Mass estimated at P12 pressure (WP12, red X), total water content (dark blue arrow) and water contents present in each phase (light blue arrows) are also given. Data from a *Fagus sylvatica* branch.

our branches, the leaf turgor loss point often occurs close to wood P12. The relationships between leaf and wood properties will be investigated more in depth in a second paper. Although we use the 'classic' three phases from TY1990, we recognise that in vivo visualisation approaches (Utsumi et al. 1996; Utsumi et al. 1998; Longuetaud et al. 2016; Longuetaud et al. 2017; Ziemińska et al. 2020) are changing our understanding of how the different processes interact with one another.

The extent of the curve covered during the third phase varied greatly from branch to branch. To standardise the extent of the third phase of the curve across branches, one extra point was estimated by assuming that the branch water content at P99 of the vulnerability curve was in equilibrium with the value of relative humidity corresponding to that water potential (as it would be if the branch were bench-dried down to P99). While the P99 differed across branches, the equilibrium relative humidity (RH_{P99}) differed by < 0.1% across samples with temperature values of 17°C–40°C, and therefore moisture content (MC) was taken to be 25.2% for all branches, based on (Ross 2010; Engelund et al. 2013):

$$RH_{P99} = e^{\left(\frac{-P99 \quad V_w}{RT}\right)},$$

$$MC = \frac{18}{M_P} + \left[\frac{K \quad RH_{P99}}{1 - K \quad RH_{P99}} + \frac{K_1 K \quad RH_{P99} + 2 \quad K_1 \quad K_2 \quad K^2 \quad RH_{P99}^2}{1 + K_1 K \quad RH_{P99} + K_1 \quad K_2 K^2 \quad RH_{P99}^2}\right],$$

where RH_{P99} is the equilibrium relative humidity at P_{99}, P_{99} is Ψ_p at 99% loss of hydraulic conductivity (MPa); V_w is partial molal volume of water ($1.8 \times 10^{-5}\,m^3\ mol^{-1}$); R is the gas constant ($8.31\,J\ K^{-1}\ mol^{-1}$); T is temperature (°C), MC is the moisture content (in %), 18 refers to molecular mass of water and $M_P = 388$, $K = 0.824$, $K_1 = 6.22$, $K_2 = 2.73$ are all empirical coefficients.

Water storage capacity (WS) is obtained as the difference between first and last branch weight measured during each of the three phases of the dehydration curve. Extensive

capacitance (C_e) is calculated from the slope of the linear regression between cumulative water loss and water potential during the first two phases of the curve or as the ratio between WS (calculated as the difference between branch mass at P12 and branch mass at equilibrium moisture content) and the difference between P12 and P99 for the third phase (Table 1). Conversely, we compare different size-normalisations to see whether they result in truly intensive properties, normalising C_e by dry mass (c_{DM}, in $gH_2O\ g^{-1}\ DM\ MPa^{-1}$), by total water content, that is, branch saturated mass minus dry branch mass (c_{TWC}, in RWC MPa^{-1}), by leaf area (c_{LA}, $gH_2O\ cm^{-2}\ MPa^{-1}$), or by water content present in each phase (c_{WC}, in RWC MPa^{-1}). Due to the absence of leaf volumes, the normalisation of the whole branch by leaf + branch volume is not tested in this study. Additionally, alternative calculations (i.e., using the following definitions: Phase I: values higher than −0.5 MPa; Phase II values between −0.1 MPa and P12; and Phase III: values lower than P12, but with the final extra point estimated by assuming that the branch was completely dry) were carried out (cf., Supporting Information: Figures S2, S3, S4, and S5 and Tables S3 and S4) to check that our conclusions are robust to assumptions regarding the employed cut-off points and definition of equilibrium wood moisture content.

2.4 | Additional Trait Measurements

At the end of the branch dehydration experiment, the branch was cut into smaller parts, and the dry mass of leaves, wood, and bark was calculated. The percentages of dry mass for each tissue type were determined by the ratio of each tissue's dry mass to the total dry mass of all tissues. To separate heartwood from sapwood, the proportion of active xylem was quantified by flowing a filtered solution dyed with toluidine blue through a wood segment, consisting of a straight fresh stem without leaves, administering the dye through the segment under gravity pressure. WD (g/cm^3, ratio of dry mass to saturated volume), was determined on a 10-cm-long stem segment cut from the bottom section of the branch. Leaf area was obtained using ImageJ by digitally scanning 10–20 needles/leaves taken from random positions within the branch to derive specific leaf area and then scaled to the branch using leaf mass. Vulnerability to embolism was measured in the Bordeaux 'CaviPlace' laboratory, following Delzon et al. (2010) and Burlett et al. (2022). Vulnerability curves were fitted to the relationship between PLC (%) and xylem pressure using the Pammenter model (Pammenter and Willigen 1998). Summary data expressed as species averages for the studied traits is included in Supporting Information: Table S6.

2.5 | Statistical Analyses

Linear mixed models were used to test the allometric relationships of WS, C_e, c_{DM}, c_{TWC}, c_{LA}, and c_{WC} with branch size. All the models (Table 2) included branch dry mass (M_{branch}) as independent variable. In addition, for the extensive properties we also tested the interaction between M_{branch} and other influencing variables (prop_heartwood, WD, P50, % leaves, % bark and % wood; one variable at a time) as fixed effects, with species and population nested within species as random effects. Capacity, capacitance and branch masses were natural log-transformed. Traits (P50 and WD) and tissue proportions (% wood, % leaves and % bark and prop_heartwood) were not transformed. We started from models with the interaction present, and simplified them until including only M_{branch}, if necessary. Notice that a significant trait effect implies that water storage changes as a function of the second variable at constant mass. Conversely, a significant trait interaction implies that the slope of the effect of mass was modified by the trait. Scaling relationships are generally examined using Model II regression approaches (e.g., standardised major axis regression). This is not done here for three reasons, that is, the hierarchical nature of the data, the use of multiple regression models and finally, the clear distinction between response variables (capacity and capacitance) versus independent variables, that is, dry mass and branch traits.

TABLE 2 | Allometry of water storage capacity (WS) and capacitance (C_e) with branch dry mass was tested using the following model: WS or C_e~ M_{branch} * factor + (1 | species/population). See legend in Table 1 for further details.

WS or C_e or c_{DM} or c_{WC} or c_{TWC} or c_{LA} ~ M_{branch}	
WS or C_e ~ M_{branch} + P50	*WS* or C_e~ M_{branch} * P50
WS or C_e ~ M_{branch} + WD	*WS* or C_e ~ M_{branch} * WD
WS or C_e ~ M_{branch} + prop_heartwood	*WS* or C_e ~ M_{branch} * prop_heartwood
WS or C_e ~ M_{branch} + % bark	WS or C_e ~ M_{branch} * % bark
WS or C_e ~ M_{branch} + % wood	WS or C_e ~ M_{branch} * % wood
WS or C_e ~ M_{branch} + % leaves	WS or C_e ~ M_{branch} * % leaves

Linear mixed-effects models were fitted using the lme4 package version 1.1.31 (Bates et al. 2015). We used the partR2 package (Stoffel, Nakagawa, and Schielzeth 2021) to estimate the standardised coefficients (ie., beta weights) and the inclusive R^2 for each fixed effect (i.e., M_{branch}, WD, P50, prop_heartwood, % bark, % leaves and % wood). Inclusive R^2 refers to the variance explained by an independent predictor in the model, both uniquely and jointly with other predictors and beta weights refer to the standardised model estimates, allowing a comparison of their relative impacts (Stoffel, Nakagawa, and Schielzeth 2021). Models with significant interactions were plotted using the interact_plot function, from the interactions package (Long and Long 2019). In Supporting Information, we also report models with an alternative approach for selection of cut-off points for each part of the curve. All statistical analysis were conducted in R software version 4.2.2 (R Core Team 2023).

3 | Results

3.1 | Allometric Relationships of Extensive Water Storage Properties Against Branch Dry Mass

We first tested the allometric relationships between extensive water storage properties and branch dry mass (Hypothesis 1). The log-log relationships between branch dry mass, water

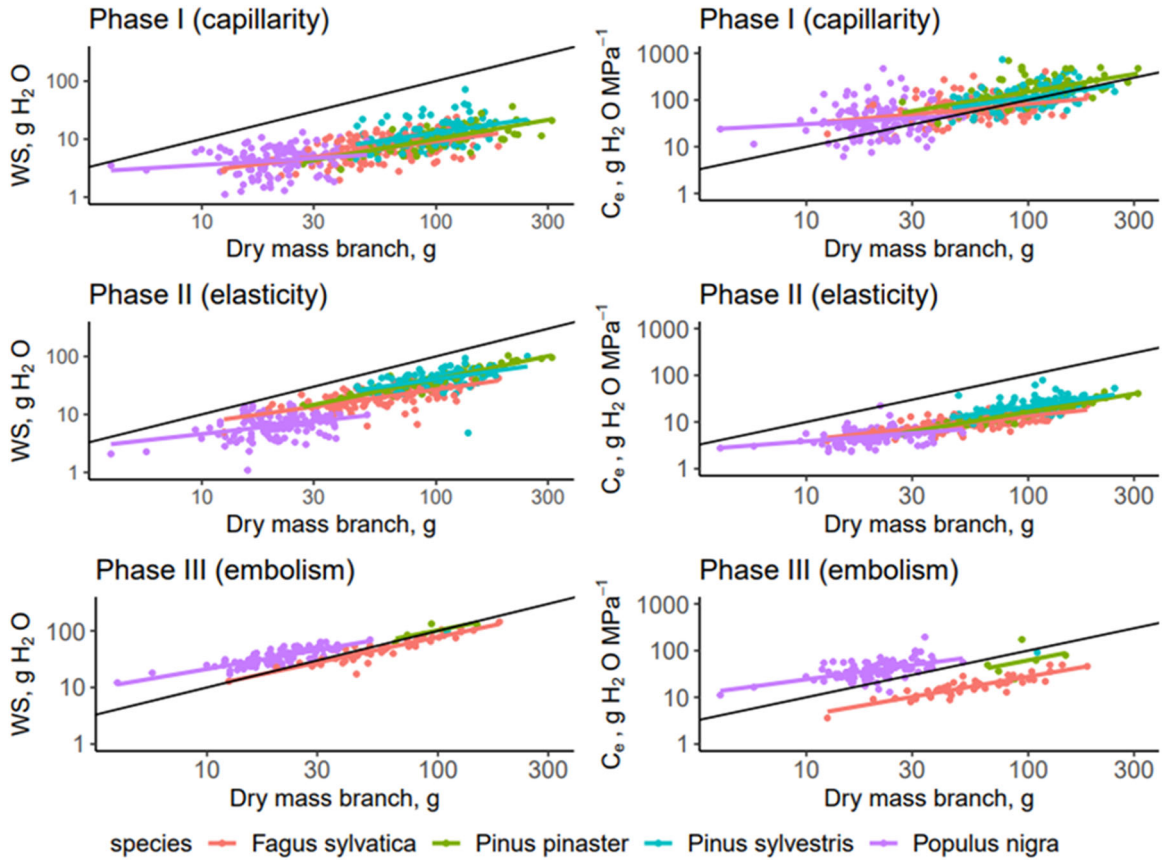

FIGURE 2 | Relationship between branch dry mass, capacity (WS) and extensive capacitance (C_e) in a log-log scale calculated for the three phases of the curve. The black line shows the 1:1 relationship (slope = 1 and intercept = 0). [Color figure can be viewed at wileyonlinelibrary.com]

storage capacity and capacitance were strongly positive for all three phases of the curve (Figure 2), although with significant intercept and slope differences across species. We generally found high values of conditional (between 0.35 and 0.96) and marginal R^2 (between 0.26 and 0.82) for models predicting WS and C_e as a function of branch mass, even though models for Phase I had lower values. The slopes for branch dry mass were lower than 1 in all cases. Without interactions, slopes in Phases I (between 0.51 and 0.57) and II (between 0.43 and 0.76) were generally lower than in Phase III (between 0.78 and 0.83), although in some cases the 95% confidence intervals overlapped among phases.

3.2 | Trait Effects on the Allometry of Extensive Water Storage Properties

To test Hypothesis 2, we examined whether other variables influenced the *allometry* of water storage properties against M_{branch}, as intercept and/or slope. Inclusive R^2 and standardised coefficients (i.e., beta weights) were always higher for M_{branch} compared to other variables (with one exception), indicating higher explanatory power and sensitivity of WS and C_e towards this variable (Tables 3 and 4; all complete models are in Supporting Information: Tables S1 and S2). M_{branch} was almost always highly significant in the multiple regressions. WD was significant for WS in Phase III but without a significant interaction with M_{branch}. P50 was significant in Phases II and III and its interaction with M_{branch} was significant in Phase II for C_e (Table 3). The prop_heartwood was significant for WS in Phase I, and its interactions with M_{branch} were significant for C_e in phase II and marginally significant for WS in Phase III (p-value = 0.053, not shown in Table 4). The % bark was significant in Phases I and III of WS and its interaction with M_{branch} was significant in Phase II of WS and C_e. The % leaves was significant in Phases I and III and its interaction with M_{branch} was significant in Phase II, both for WS and C_e. The % wood was significant in all three phases of WS and in Phase III of C_e, although its interactions with M_{branch} were not significant.

Finally, slope analysis was employed to explore the direction of the significant interactions between M_{branch} and other variables (Figures 3 and 4 and Supporting Information: Figures S4 and S5), by plotting the effects of high (+ 1 SD), average (mean) and low (−1 SD) values of the variable. For WS (Figure 3 and Supporting Information: Figure S4), lower % bark and higher % leaves in Phase II increased the M_{branch} slope. For C_e (Figure 4 and Supporting Information: Figure S5), decreased (more negative) P50 decreased the M_{branch} slope, while prop_heartwood, lower % bark and higher % leaves all increased the M_{branch} slope in Phase II.

All results obtained using the alternative approach (Supporting Information) were consistent with the main results with only a few exceptions, i.e., the interactions of M_{branch} with prop_heartwood and P50 were significant in phase III.

TABLE 3 | Linear mixed model results of the tests of the effects of branch dry mass and the traits Wood density (WD) and P50 on capacity and extensive capacitance. The table includes the coefficients (Coeff.), with the *p*-values significance (Sig., significance codes: 0'***' 0.001 '**',0.01 '*'0.05 'ns') and with confidence intervals of 95% (CI). It also includes the standardised coefficients (stand. coeff., i.e., beta weights), conditional R^2 (R^2-C), marginal R^2 (R^2-M), and inclusive R^2 (IR^2) for each factor of the model. Branch mass, WS and capacitance were log transformed, WD and P50 were not.

WS g H_2O	Phase I: Capillarity				Phase II: Elasticity				Phase III: Embolism + Residual water			
Model	Coeff. | Sig. (CI)	Stand. Coeff.	R^2-C (R^2-M)	IR^2	Coeff. | Sig. (CI)	Stand. Coeff.	R^2-C (R^2-M))	IR^2	Coeff. | Sig. (CI)	Stand. Coeff.	R^2-C (R^2-M)	IR^2
M_{branch}	0.57*** (0.48–0.66)	0.67	0.70 (0.47)	0.47	0.63*** (0.55–0.71)	0.55	0.80 (0.43)	0.43	0.82*** (0.76–0.88)	1.24	0.94 (0.80)	0.79
WD	—	—	—	—	—	—	—	—	−0.70 * (−1.33 to −0.13)	−0.11		0.14
M_{branch} * WD	—	—	—	—	—	—	—	—	—	—	—	—
M_{branch}	0.57*** (0.48–0.66)	0.67	0.70 (0.47)	0.47	0.64*** (0.57–0.72)	0.56	0.85 (0.80)	0.75	0.82*** (0.77-0.88)	1.24	0.94 (0.77)	0.74
P50	—	—	—	—	−0.45*** (−0.57 to 0.35)	−0.34		0.66	0.22*** (0.11-0.33)	0.29		0.31
M_{branch} * P50	—	—	—	—	—	—	—	—	—	—	—	—
C_e g H_2O MPa^{-1}	**Phase I. Capillarity**				**Phase II: Elasticity**				**Phase III: Embolism + Residual water**			
Model	Coeff. | Sig. (CI)	Stand. Coeff.	R^2-C (R^2-M)	IR^2	Coeff. | Sig. (CI)	Stand. Coeff.	R^2-C (R^2-M)	IR^2	Coeff. | Sig. (CI)	Stand. Coeff.	R^2-C (R^2-M)	IR^2
M_{branch}	0.51*** (0.37–0.67)	0.47	0.46 (0.26)	0.26	0.64*** (0.57-0.71)	0.74	0.80 (0.65)	0.65	0.78*** (0.66–0.90)	0.90	0.89 (0.36)	0.36
WD	—	—	—	—	—	—	—	—	—	—	—	—
M_{branch} * WD	—	—	—	—	—	—	—	—	—	—	—	—
M_{branch}	0.51*** (0.37–0.67)	0.47	0.46 (0.26)	0.26	0.17 ns (−0.09 to 0.44)	0.20	0.81 (0.65)	0.65	0.80*** (0.68–0.91)	0.92	0.85 (0.29)	0.26
P50	—	—	—	—	0.52** (0.17–0.86)	0.52		0.40	0.36** (0.14–0.58)	0.35		0.07
M_{branch} * P50	—	—	—	—	−0.15 *** (−0.23 to 0.07)	−1.01		0.59	—	—	—	—

TABLE 4 | Linear mixed model results of the tests of the effects of branch dry mass and of the heartwood ratio (prop_heartwood) and tissue percentages (%bark, %leaves and %wood) on capacity (WS) and extensive capacitance (C_e). The table includes the coefficients (Coeff.), with the *p*-values' significance (Sig., significance codes: 0'***' 0.001 '**'0.01 '*'0.05 'ns') and with confidence intervals of 95% (CI). It also includes the standardised coefficients (stand. coeff., i.e., beta weights), conditional R^2 (R^2-C), marginal R^2 (R^2-M) and inclusive R^2 (IR^2) for each factor of the model. Branch mass, WS and capacitance were log transformed, % tissues were not.

WS g H_2O	Phase I. Capillarity				Phase II: Elasticity				Phase III: Embolism + Residual water			
Model	Coeff. | Sig. (CI)	Stand. Coeff.	R^2-C (R^2-M)	IR^2	Coeff. | Sig. (CI)	Stand. Coeff.	R^2-C (R^2-M)	IR^2	Coeff. | Sig. (CI)	Stand. Coeff.	R^2-C (R^2-M)	IR^2
M_{branch}	0.57***	0.68	0.70	0.48	0.63***	0.55	0.80	0.43	0.82***	1.24	0.95	0.78
prop_heartwood	(0.48–0.65)	0.08	(0.49)	0.03	(0.55–0.71)	–	(0.43)	–	(0.76–0.88)	–	(0.78)	–
M_{branch}	0.42*	–		–	–	–	–	–	–	–	–	–
*prop_heartwood	(0.10–0.76)				–		–		–		–	
	–											
M_{branch}	0.55 ***	0.65	0.72	0.50	0.74***	0.65	0.80	0.48	0.83***	1.25	0.96	0.77
% bark	(0.46–0.64)	−0.11	(0.50)	0.23	(0.60–0.89)	0.15	(0.49)	0.23	(0.77–0.88)	−0.15	(0.78)	0.21
M_{branch} *% bark	−0.01*	–	–	–	0.02 ns (−0.01	−0.20		0.03	−0.01*** (−0.01	–	–	–
	(−0.02 to −0.00)				to −0.04)				to −0.01)			
	–				−0.01* (−0.01				–			
					to −0.00)							
M_{branch}	0.56***	0.66	0.71	0.45	0.43***	0.37	0.81	0.43	0.83***	1.25	0.95	0.78
% leaves	(0.47–0.65)	0.15	(0.47)	0.03	(0.24–0.62)	0.15	(0.46)	0.04	(0.77–0.88)	0.20	(0.80)	0.01
M_{branch} *% leaves	0.01**	–	–	–	−0.01 ns	0.35		0.26	0.01***	–	–	–
	(0.00–0.01)				(−0.02-0.00)				(0.00-0.01)			
	–				0.00*				–			
					(0.00–0.01)							
M_{branch}	0.57***	0.68	0.70	0.41	0.63***	0.55	0.81	0.38	0.82***	1.24	0.94	0.78
% wood	(0.48–0.66)	−0.16	(0.44)	0.00	(0.56–0.71)	0.11	(0.40)	0.00	(0.76–0.88)	−0.29	(0.82)	0.10
M_{branch} *% wood	−0.01* (−0.01	–	–	–	−0.01*	–	–	–	−0.01*** (−0.02	–	–	–
	to −0.00)				(−0.01—0.00)				to −0.00)			
	–				–				–			

C_e g H_2O MPa^{-1}	Phase I. Capillarity				Phase II: Elasticity				Phase III: Embolism + Residual Water			
Model	Coeff. | Sig. (CI)	Stand. Coeff.	R^2-C (R^2-M)	IR^2	Coeff. | Sig. (CI)	Stand. Coeff.	R^2-C (R^2-M)	IR^2	Coeff. | Sig. (CI)	Stand. Coeff.	R^2-C (R^2-M)	IR^2
M_{branch}	0.51***	0.47	0.48	0.26	0.67***	0.79	0.81	0.65	0.78***	0.90	0.89	0.36
prop_heartwood	(0.37–0.66)	0.10	(0.27)	0.03	(0.61–0.75)	0.28	(0.65)	0.02	(0.66–0.90)	–	(0.36)	–
M_{branch} *	0.70**	–		–	1.55**	−0.28		0.06	–	–	–	–
prop_heartwood	(0.17–1.22)				(0.45–2.64)				–		–	
	–				−0.35**							
					(−0.60 to −0.09)							

(Continues)

TABLE 4 | (Continued)

WS g H_2O	Phase I. Capillarity				Phase II: Elasticity				Phase III: Embolism + Residual water			
Model	Coeff. | Sig. (CI)	Stand. Coeff.	R^2-C (R^2-M)	IR^2	Coeff. | Sig. (CI)	Stand. Coeff.	R^2-C (R^2-M)	IR^2	Coeff. | Sig. (CI)	Stand. Coeff.	R^2-C (R^2-M)	IR^2
M_{branch}	0.51***	0.47	0.46	0.26	0.76***	0.89	0.83	0.66	0.78***	0.90	0.89	0.36
% bark	(0.37–0.67)	–	(0.26)	–	(0.65–0.88)	0.21	(0.68)	0.35	(0.66–0.90)	–	(0.36)	–
M_{branch} *% bark	–	–	–	–	0.02 ns (−0.00 to 0.04)	0.31		0.05	–	–	–	–
	–		–		−0.01** (−0.01 to −0.00)				–		–	
M_{branch}	0.53***	0.49	0.46	0.28	0.46***	0.53	0.83	0.58	0.79***	0.91	0.88	0.36
% leaves	(0.40–0.74)	0.19	(0.32)	0.04	(0.31–0.61)	−0.13	(0.63)	0.06	(0.67–0.91)	0.14	(0.37)	0.01
M_{branch} *% leaves	0.01** (0.00–0.02)	–	–	–	−0.01 ns (−0.02 to 0.01)	0.40		0.36	0.01* (0.00–0.01)	–	–	–
	–				0.00* (0.00–0.01)				–			
M_{branch}	0.51***	0.47	0.46	0.26	0.64***	0.74	0.80	0.65	0.79***	0.91	0.84	0.33
% wood	(0.37–0.67)	–	(0.26)	–	(0.57–0.71)	–	(0.65)	–	(0.67–0.91)	−0.34	(0.39)	0.02
M_{branch} *% wood	–	–	–	–	–	–	–	–	−0.02** (−0.02 to −0.01)	–	–	–
	–		–		–		–		–			

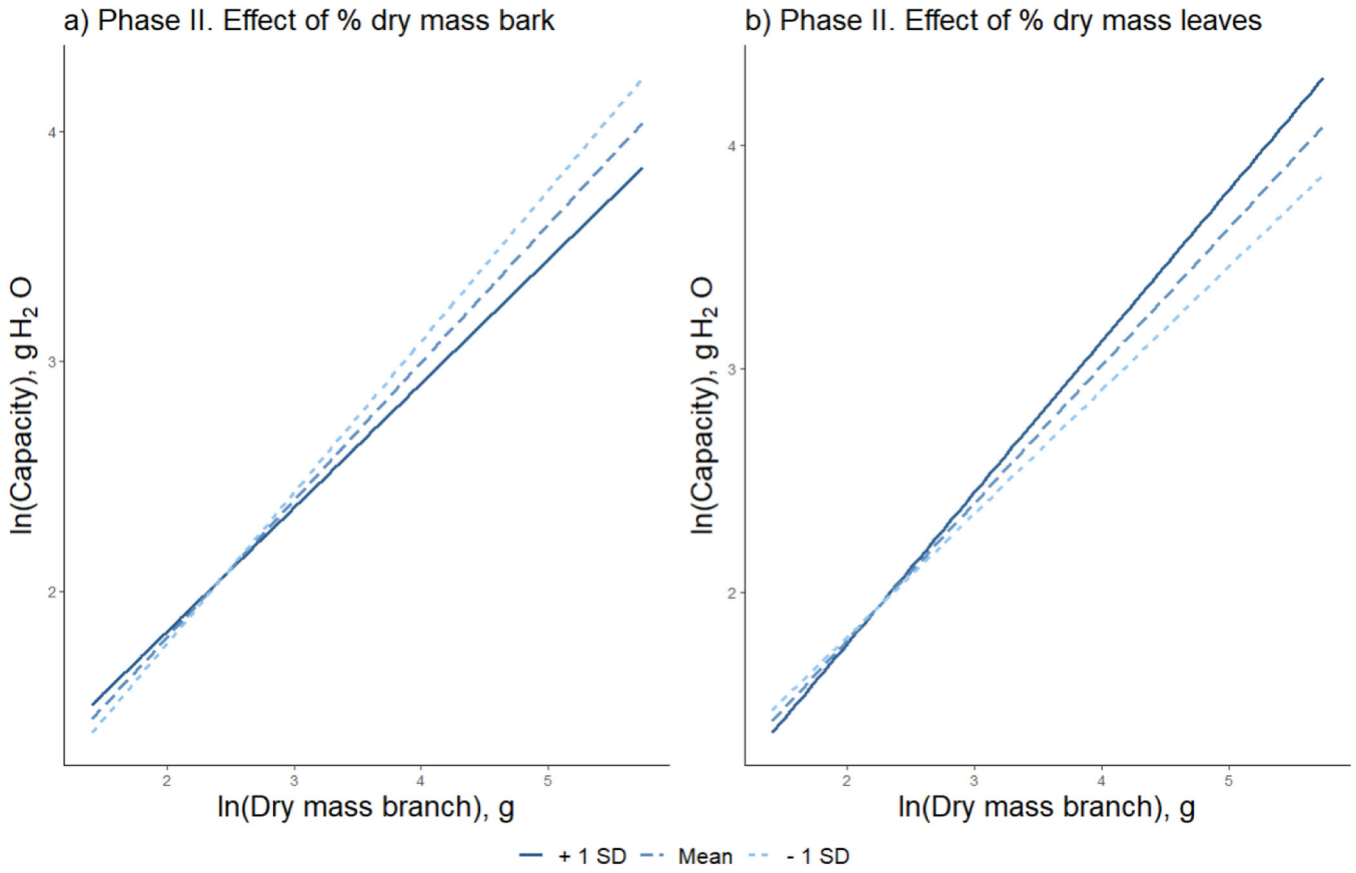

FIGURE 3 | Plots of interactions between dry mass branch (M_{branch}) and (a) %bark, and (b) % leaves for the models of capacity (WS) on a natural-log transformed scale, using the model: ln(WS) ~ ln(M_{branch}) * trait + (1| species/Population). [Color figure can be viewed at wileyonlinelibrary.com]

3.3 | Allometric Relationships of Size-Normalised Capacitance

Finally, to test Hypothesis 3, we compared the mass dependency of size-normalised properties (c_{DM}, c_{TWC}, c_{LA}, and c_{WC}) across the three distinct phases (Table 5 and Supporting Information: Figure S6). Normalising extensive capacitance using branch-level properties (i.e., branch dry mass, leaf area or total water content), the slopes against branch dry mass were now negative (significantly lower from zero) in all cases, except for Phase III in c_{TWC}, indicating quasi-asymptotic relationships. Conversely, normalising capacitance using the water content available in each of the three phases, the slopes for M_{branch} were not significantly different from zero for any of the three phases.

4 | Discussion

4.1 | Water Storage Properties Change Allometrically With Branch Dry Mass

Coefficients lower than 1 support allometric (quasi-asymptotic) relationships of branch capacity and extensive capacitance with size across the distinct phases of the water release curve. The nature of the allometric relationship of extensive water storage properties with branch mass has not been investigated previously, at least to our knowledge. Significant effects of tree size on capacitance and water storage capacity were reported in previous works, with larger trees having higher stem intensive capacitance (Phillips et al. 1997; Meinzer, James, and Goldstein 2004; Scholz et al. 2011). Our results point to the opposite direction, with slopes of the extensive properties always < 1 and hence slopes < 0 against mass for the intensive properties. Slopes of extensive properties against mass varied between 0.43 and 0.83, and mostly between 0.5 and 0.75, that is, including the ½, ⅔ and the ¾ slopes. A detailed analysis of the congruence of our slopes against these theoretical slopes was not attempted here, also given that Model II regression was not employed. We simply note that the ⅔ slope obtained with maximum likelihood regression is broadly consistent with the scaling of the ratio of surface losses to internal water volumes.

4.2 | Traits and Mass Fractions Affect the Allometry of Water Storage

According to our second hypothesis, allometry of extensive properties is explained by how variables related to water storage, such as tissues proportions, WD and xylem vulnerability to embolism change with mass. When WD was significant, branches with less dense wood had higher values of WS, as expected from the trade-off occurring in saturated branches between the space available for water storage and the space occupied by cell walls, similar to other reports (e.g., Dlouhá et al. 2018; Li et al. 2018; Wolfe and Kursar 2015; Ziemińska et al. 2020; O'Keefe et al. 2023). Some studies (Utsumi et al. 1996; Utsumi

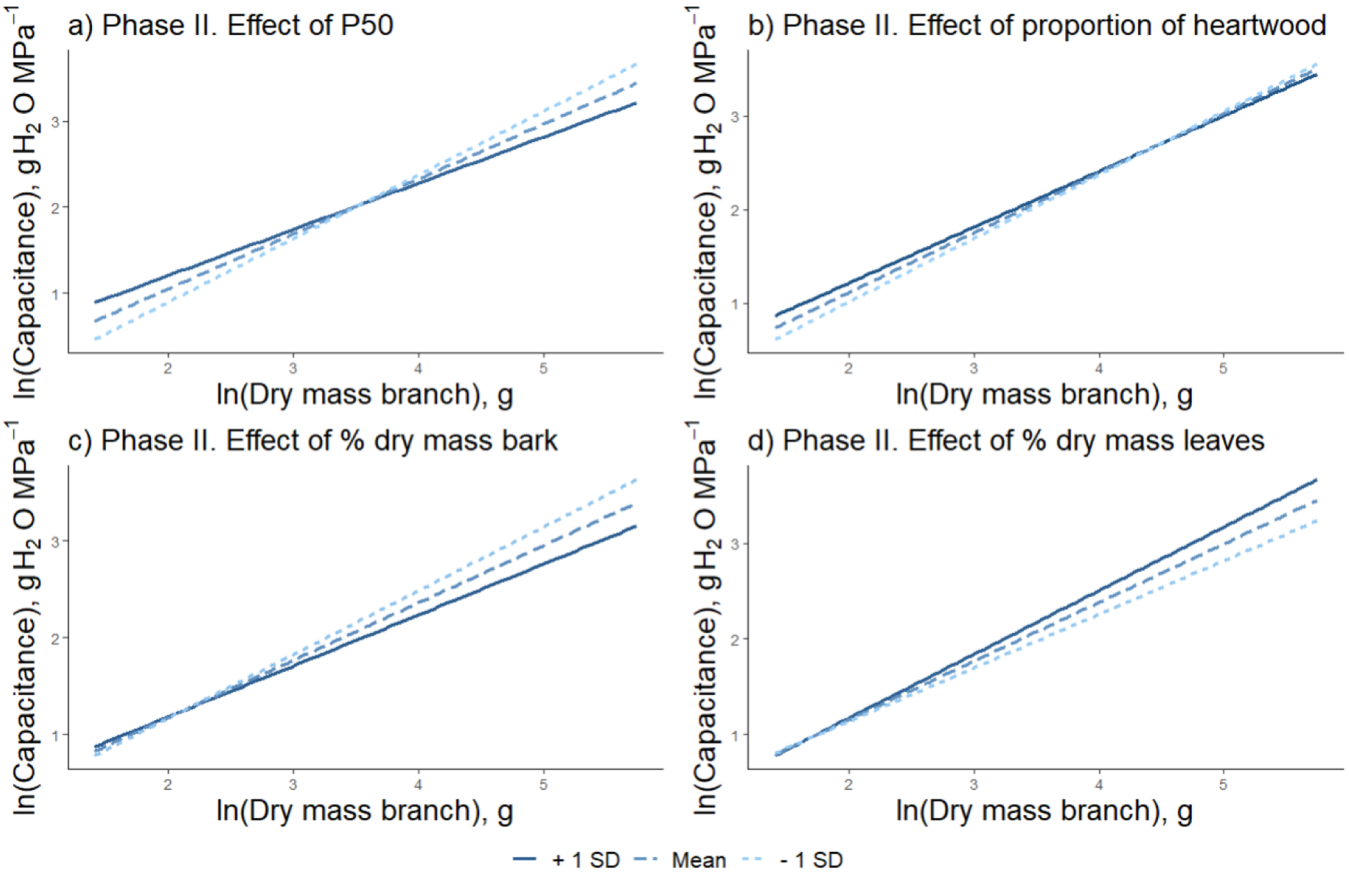

FIGURE 4 | Plots of interactions between dry mass branch (M_{branch}) and a) P50, b) %heartwood, c) %bark, and d) %leaves for the models of extensive capacitance (C_e) on a natural-log transformed scale, using the model: $\ln(C_e) \sim \ln(M_{branch})$ * trait + (1| species/Population). [Color figure can be viewed at wileyonlinelibrary.com]

TABLE 5 | Linear mixed model results of the significance of the branch dry mass coefficients for intensive capacitances. The table includes the dry mass branch coefficients (M_{branch} Coeff.), with *p*-values' significance (Sig., significance codes: 0'***' 0.001 '**'0.01 '*'0.05 'ns') and with confident intervals of 95% (CI). It also includes the conditional R^2 (R^2-C) and marginal R^2 (R^2-M) of the model.

Intensive capacitances Units		**c_{DM} g H_2O g^{-1} MPa^{-1}**	**c_{TWC} RWC MPa^{-1}**	**c_{LA} g H_2O cm^{-2} MPa^{-1}**	**c_{WC} RWC MPa^{-1}**
Phase I:	M_{branch}Coeff.	−0.49***	−0.27 ***	−0.59***	−0.01 ns
Capillarity	CI	(−0.63 to −0.33)	(−0.40 to −0.09)	(−0.76 to −0.43)	(−0.14 to 0.12)
	R^2-M	0.24	0.10	0.15	0.00
	R^2-C	0.45	0.30	0.73	0.20
Phase II:	M_{branch}Coeff.	−0.36***	−0.21***	−0.38***	−0.01 ns
Elasticity	CI	(−0.43 to −0.29)	(−0.26 to −0.15)	(−0.46 to −0.28)	(−0.08 to 0.05)
	R^2-M	0.37	0.17	0.09	0.00
	R^2-C	0.65	0.64	0.85	0.58
Phase III:	M_{branch}Coeff.	−0.22***	−0.01 ns	−0.37***	−0.03 ns
Embolism	CI	(−0.34 to −0.10)	(−0.12 to 0.10)	(−0.57 to −0.17)	(−0.15 to 0.09)
	R^2-M	0.04	0.00	0.07	0.00
	R^2-C	0.83	0.77	0.73	0.47

et al. 1998; Longuetaud et al. 2016; Longuetaud et al. 2017; Ziemińska et al. 2020) show that some cell lumen volume in wood can be totally or partially empty in certain circumstances, and therefore not contribute to storage. If so, the finding that WD was rarely a significant explanatory variable is consistent with a limited role for this trade-off. The interaction between WD and branch dry mass was also never significant, supporting the inference that allocation to intercellular space versus cell

walls did not change as the branches grew in mass. Consistent with this result, WD did not scale with branch dry mass (Supported Information: Table S5).

The effect of P50 was significant only as an intercept in WS and its sign shifted from negative to positive between Phases II and III. A less negative P50 was associated with lower WS during the elastic phase but higher WS during the embolism phase, as expected from the fact that the transition between the two phases was defined based on P12. In general, this result is consistent with the trade-off between the amount of water released to support canopy transpiration under non-extreme drought and drought tolerance as determined by resistance to xylem embolism (Meinzer et al. 2009; O'Keefe et al. 2023). The results were similar for C_e. However, in this case the significant interaction with P50 during Phase II implied that the trade-off mentioned above was mass dependent. Greater vulnerability was associated with higher Phase II capacitance in small branches but corresponded to lower Phase II capacitance in large branches. In Phase III, the interaction between P50 and dry mass on C_e was not significant. Overall, these results are also consistent with the reported trade-off between resistance to embolism and capacitance (Mcculloh et al. 2014), although other studies did not find evidence for this trade-off (Gleason et al. 2014). Additionally, the limited number of data points at the end of the curve and the use of only four species could explain why P50 did not influence this final phase in our study.

Interestingly, when prop_heartwood was significant, a lower heartwood ratio was associated with higher slope of WS (Phase I only) and C_e (Phases I and II). A significant interaction term for Phase II of C_e also implies that as mass increases, the amount of Phase II water increases as the prop_heartwood decreases, suggesting that heartwood water was not released during Phases I and II. Nonetheless, prop_heartwood did not scale significantly with branch mass in our data, a somewhat surprising result. The results above reflect the observed variance across branches, but using a wider range of branch sizes would have likely resulted in stronger effects. Contrary to expectations, the effects of heartwood ratio were not apparent during Phase III, suggesting that water release from heartwood was probably not insignificant during this phase. It should be noted, however, that our calculations for the final part of the curve may have over-estimated the water available for WS and C_e.

When % leaves was significant, a higher % leaves was associated with higher WS and C_e. Considering Phase II, higher values of WS and C_e in branches with a higher proportion of leaf mass imply that with a greater proportion of leaf mass, more water is released during the elasticity phase. It may also imply that leaves release water more rapidly than the rest of tissues (Beckett et al. 2024).

The trends for % leaves were reversed when % bark was examined. When % bark was significant, a lower % bark was associated with higher WS and C_e. A higher slope on branches with a lower proportion of bark mass implies that as mass increases, the available water increases as the % bark decreases during the elasticity phase. Because % bark scaled negatively with branch dry mass, the two effects reinforce each other. Larger branches have less % bark and having lower % bark increases the allometric slope. It would therefore appear that bark water storage is limited to short terminal branches where both effects are small. This contrasts with the argument that bark provides a significant water store for capacitance in large branches thanks to its elastic cellular properties (e.g., Pfautsch, Hölttä, and Mencuccini 2015).

These results suggest that at the beginning of dehydration, not all stored water may in fact be available to be released. As branch dehydration progresses, bark, sapwood and heartwood may lose less water proportionally than leaves. Upon reaching embolism, all left-over water may become available (Beckett et al. 2024).

Overall, our results confirm the relevance of already proposed trade-offs, with respect to the roles of WD and P50. In addition, we show that additional trade-offs exist related to tissue fractions (sapwood/heartwood and leaf/bark/wood fractions). These trade-offs only become apparent if an allometric approach is taken across a range of branch sizes. Overall, P50 and the leaf fraction emerge as the most important variables, with the role of leaf capacitance during the elastic phase and water release following embolism during the final phase likely dependent on these properties.

4.3 | Allometric Relationships of Size-Normalised Capacitance and Branch-Level Traits

When extensive capacitance is normalised by branch dry mass or leaf area or total water content, the coefficients expressing size-dependency remain significant, therefore (negative) allometry persists. However, when C_e is normalised by the water content present in each phase, the coefficients expressing size-dependency become non-significant, such that allometry disappears and a size-independent property (in effect, a branch-level trait) is obtained. These results support the TY1990 model, that branch capacitance is given by a mix of functionally different pools of water, in agreement with our third hypothesis. Using rehydration, as opposed to dehydration curves, previous research documented biphasic recharge in the stem (O'Keefe et al. 2023), also implying that capacitance is constituted by different pools of water. Our results at the branch scale are also consistent with results at the leaf scale, whereby leaf capacitance is calculated separately pre- and post-turgor loss point, albeit employing total water content for both cases, again because of differences in the processes involved.

Implicitly assuming a single functional pool of water is especially inappropriate across a large range of branch sizes, because the importance of the processes accessing the different pools vary with branch size. Consequently, the only effective way to standardise branch-level capacitance and obtain a size-independent trait and intensive property is to normalise it relative to the water available in each phase.

4.4 | Implications for Allometric Predictions and Modelling

Our study carries three main implications for modelling purposes. Firstly, each branch is characterised by one capacitance value for each phase, similarly to the case for leaves, but with limits among phases estimated from capillarity (between −0.2

and −0.5 MPa), and the parameters of the xylem vulnerability curve. Secondly, values of WS and (extensive) capacitance can be estimated from branch size. Our preliminary results suggest that allometric slopes against dry mass of between 0.50 and 0.70 are appropriate for all three phases of WS and C_e. Thirdly, accurate estimates of capacitance need to account for declining leaf mass fraction in larger branches, consistent with how variations in carbon allocation to various plant structures can affect water retention approaches. In future research, selecting the best normalisation scheme of capacitance may be crucial to model capacitance at branch, tree and ecosystem scales. Further work is required to test how the branch-level results presented here can be scaled to entire trees.

5 | Conclusions

Water storage capacity and capacitance show allometric relationships with branch dry mass, influenced by distinct variables. For Phase I, characterised by capillarity, there is no evidence of factors affecting the allometric exponent on capacity and capacitance, although water storage at constant mass can vary depending on proportion of heartwood, leaves, bark and wood. In Phase II, characterised by elasticity, the most significant influences on water storage capacity and capacitance appear to be the proportions of leaves and bark. Additionally, the heartwood ratio and P50 (representing xylem vulnerability) impact the allometric relationships of capacitance. Overall, changes in xylem vulnerability and tissue proportions, such as leaves, bark or heartwood, play a significant role as the branch grows in mass, while variables such as intercellular space allocation (mediated by WD) and changes in wood proportions showed a low importance. These results support the TY1990 model and the existence of different branch water pools. Normalising capacitance by the relevant range of water contents results in a size-independent branch-level trait that could be applied in comparative and modelling studies.

Acknowledgements

The authors acknowledge all staff involved in field sampling and laboratory measurements (special mention to CREAF-URFM field/lab teams). This study was supported by EU-2020 programme via grant 862221 (ForGenIUs). The authors thank the Agència de Gestió d'Ajuts Universitaris i de Recerca de Catalunya (grant 2021 SGR 00849). SH received a predoctoral fellowship (PRE2021-098897) funded by MCIN/AEI/10.13039/501100011033 and European Social Fund (ESF+), within the Severo Ochoa Centre of Excellence grant (CEX2018-000828-S). OB received a postdoctoral Junior Leader fellowship provided by "la Caixa" Foundation. JM-V benefited from an ICREA Academia award (Institució Catalana de Recerca i Estudis Avançats).

Data Availability Statement

The data that support the findings of this study are available from the corresponding author upon reasonable request.

References

Aparecido, L. M. T., G. R. Miller, A. T. Cahill, and G. W. Moore. 2016. "Comparison of Tree Transpiration Under wet and dry Canopy Conditions in a Costa Rican Premontane Tropical Forest." *Hydrological Processes* 30, no. 26: 5000–5011.

Bates, D., M. Mächler, B. Bolker, and S. Walker. 2015. "Fitting Linear Mixed-Effects Models Using Lme4." *Journal of Statistical Software* 67, no. 1: 1–48.

Beckett, H. A. A., C. Bryant, T. Neeman, M. Mencuccini, and M. C. Ball. 2024. "Plasticity in Branch Water Relations and Stem Hydraulic Vulnerability Enhances Hydraulic Safety in Mangroves Growing Along a Salinity Gradient." *Plant, Cell & Environment* 47, no. 3: 854–870.

Blackman, C. J., S. Pfautsch, B. Choat, S. Delzon, S. M. Gleason, and R. A. Duursma. 2016. "Toward an Index of Desiccation Time to Tree Mortality Under Drought." *Plant, Cell & Environment* 39, no. 10: 2342–2345.

Brodribb, T. J., and N. M. Holbrook. 2003. "Stomatal Closure During Leaf Dehydration, Correlation With Other Leaf Physiological Traits." *Plant Physiology* 132, no. 4: 2166–2173.

Bryant, C., T. I. Fuenzalida, N. Brothers, et al. 2021. "Shifting Access to Pools of Shoot Water Sustains Gas Exchange and Increases Stem Hydraulic Safety During Seasonal Atmospheric Drought." *Plant, Cell & Environment* 44, no. 9: 2898–2911.

Burlett, R., C. Parise, G. Capdeville, et al. 2022. "Measuring Xylem Hydraulic Vulnerability for Long-Vessel Species: An Improved Methodology With the Flow Centrifugation Technique." *Annals of Forest Science* 79, no. 1: 5.

Delzon, S., C. Douthe, A. Sala, and H. Cochard. 2010. "Mechanism of Water-Stress Induced Cavitation in Conifers: Bordered Pit Structure and Function Support the Hypothesis of Seal Capillary-Seeding." *Plant, Cell & Environment* 33, no. 12: 2101–2111.

Dlouhá, J., T. Alméras, J. Beauchêne, B. Clair, and M. Fournier. 2018. "Biophysical Dependences Among Functional Wood Traits." *Functional Ecology* 32, no. 12: 2652–2665.

Domec, J. C., and B. L. Gartner. 2001. "Cavitation and Water Storage Capacity in Bole Xylem Segments of Mature and Young Douglas-Fir Trees." *Trees* 15: 204–214.

Engelund, E. T., L. G. Thygesen, S. Svensson, and C. A. S. Hill. 2013. "A Critical Discussion of the Physics of Wood-Water Interactions." *Wood Science and Technology* 47: 141–161.

Gleason, S. M., C. J. Blackman, A. M. Cook, C. A. Laws, and M. Westoby. 2014. "Whole-Plant Capacitance, Embolism Resistance and Slow Transpiration Rates All Contribute to Longer Desiccation Times in Woody Angiosperms From Arid and Wet Habitats." *Tree Physiology* 34, no. 3: 275–284.

Hartzell, S., M. S. Bartlett, and A. Porporato. 2017. "The Role of Plant Water Storage and Hydraulic Strategies in Relation to Soil Moisture Availability." *Plant and Soil* 419: 503–521.

Holbrook, M. N. 1995. "Stem Water Storage." In *Plant Stems*. New York: Academic Press.

Hölttä, T., H. Cochard, E. Nikinmaa, and M. Mencuccini. 2009. "Capacitive Effect of Cavitation in Xylem Conduits: Results From a Dynamic Model." *Plant, Cell & Environment* 32, no. 1: 10–21.

Hu, G., H. Liu, H. Shangguan, X. Wu, X. Xu, and M. Williams. 2018. "The Role of Heartwood Water Storage for Sem-Arid Trees under Drought." *Agricultural and Forest Meteorology* 256–257: 534–541.

Jupa, R., L. Plavcová, V. Gloser, and S. Jansen. 2016. "Linking Xylem Water Storage With Anatomical Parameters in Five Temperate Tree Species." *Tree Physiology* 36, no. 6: 756–769.

Li, X., C. J. Blackman, B. Choat, et al. 2018. "Tree Hydraulic Traits Are Coordinated and Strongly Linked to Climate-Of-Origin Across a Rainfall Gradient." *Plant, Cell & Environment* 41, no. 3: 646–660.

Long, J. A., and M. J. A. Long. 2019. "Package 'interactions'." https://cran.r-project.org/package=interactions.

Longuetaud, F., F. Mothe, M. Fournier, J. Dlouha, P. Santenoise, and C. Deleuze. 2016. "Within-Stem Maps of Wood Density and Water

Content for Characterization of Species: a Case Study on Three Hardwood and Two Softwood Species." *Annals of Forest Science* 73: 601–614.

Longuetaud, F., F. Mothe, P. Santenoise, et al. 2017. "Patterns of Within-Stem Variations in Wood Specific Gravity and Water Content for Five Temperate Tree Species." *Annals of Forest Science* 74: 64.

Mantova, M., S. Herbette, H. Cochard, and J. M. Torres-Ruiz. 2022. "Hydraulic Failure and Tree Mortality: From Correlation to Causation." *Trends in Plant Science* 27, no. 4: 335–345.

Martin-StPaul, N., S. Delzon, and H. Cochard. 2017. "Plant Resistance to Drought Depends on Timely Stomatal Closure." *Ecology Letters* 20, no. 11: 1437–1447.

Mcculloh, K. A., D. M. Johnson, F. C. Meinzer, and D. R. Woodruff. 2014. "The Dynamic Pipeline: Hydraulic Capacitance and Xylem Hydraulic Safety in Four Tall Conifer Species." *Plant, Cell & Environment* 37, no. 5: 1171–1183.

Meinzer, F. C., S. A. James, and G. Goldstein. 2004. "Dynamics of Transpiration, sap Flow and use of Stored Water in Tropical Forest Canopy trees." *Tree Physiology* 24: 901–909.

Meinzer, F. C., S. A. James, G. Goldstein, and D. Woodruff. 2003. "Whole-Tree Water Transport Scales With Sapwood Capacitance in Tropical Forest Canopy Trees." *Plant, Cell & Environment* 26, no. 7: 1147–1155.

Meinzer, F. C., D. M. Johnson, B. Lachenbruch, K. A. McCulloh, and D. R. Woodruff. 2009. "Xylem Hydraulic Safety Margins in Woody Plants: Coordination of Stomatal Control of Xylem Tension With Hydraulic Capacitance." *Functional Ecology* 23, no. 5: 922–930.

Meinzer, F. C., D. R. Woodruff, J. C. Domec, et al. 2008. "Coordination of Leaf and Stem Water Transport Properties in Tropical Forest Trees." *Oecologia* 156: 31–41.

Muggeo, V. M., and M. V. M. Muggeo. 2017. "Package 'Segmented'." *Biometrika* 58, no. 525: 516–534.

Mc Naught, A. D., and A. Wilkinson. 2014. *IUPAC. Compendium of Chemical Terminology* (2nd ed. The "Gold Book"). Oxford: Blackwell Science. https://goldbook.iupac.org/.

Niklas, K. J. 2004. "Plant Allometry: Is There a Grand Unifying Theory?" *Biological Reviews* 79, no. 4: 871–889.

O'Keefe, K., D. D. Smith, and K. A. McCulloh. 2023. "Linking Stem Rehydration Kinetics to Hydraulic Traits Using a Novel Method and Mechanistic Model." *Annals of Botany* 131, no. 7: 1121–1131.

Pammenter, N. W., and W. C. Vander. 1998. "A Mathematical and Statistical Analysis of the Curves Illustrating Vulnerability of Xylem to Cavitation." *Tree Physiology* 18: 589–593.

Pérez Cordero, L. D., and M. Kanninen. 2003. "Heartwood, Sapwood and Bark Content, and Wood Dry Density of Young and Mature Teak (Tectona grandis) Trees Grown in Costa Rica." *Silva Fennica* 37, no. 1: 45–54.

Pfautsch, S., T. Hölttä, and M. Mencuccini. 2015. "Hydraulic Functioning of Tree Stems - Fusing Ray Anatomy, Radial Transfer and Capacitance." *Tree Physiology* 35, no. 7: 706–722.

Phillips, N., A. Nagchaudhuri, R. Oren, and G. Katul. 1997. "Time Constant for Water Transport in Loblolly Pine Trees Estimated From Time Series of Evaporative Demand and Stem Sapflow." *Trees* 11: 412–419.

Pivovaroff, A. L., R. Burlett, B. Lavigne, H. Cochard, L. S. Santiago, and S. Delzon. 2016. "Testing the 'Microbubble Effect' Using the Cavitron Technique to Measure Xylem Water Extraction Curves." *AoB Plants* 8: 1–10.

Pratt, R. B., A. L. Jacobsen, M. I. Percolla, M. E. De Guzman, C. A. Traugh, and M. F. Tobin. 2021. "Trade-Offs Among Transport, Support, and Storage in Xylem From Shrubs in a Semiarid Chaparral Environment Tested with Structural Equation Modeling." *Proceedings of the National Academy of Sciences of the United States of America* 118, no. 33: e2104336118.

R Core Team2023. *R: A Language and Environment for Statistical Computing: Open Journal of Statistics*. Vienna: R Foundation for Statistical Computing.

Ross, R. 2010. *Wood Handbook: Wood as an Engineering Material*. Madison: USDAFS.

Ruffault, J., F. Pimont, H. Cochard, J. L. Dupuy, and N. Martin-Stpaul. 2022. "Sureau-Ecos v2.0: A Trait-Based Plant Hydraulics Model for Simulations of Plant Water Status and Drought-Induced Mortality at the Ecosystem Level." *Geoscientific Model Development* 15, no. 14: 5593–5626.

Scholz, F. G., S. J. Bucci, G. Goldstein, F. C. Meinzer, A. C. Franco, and F. Miralles-wilhelm. 2007. "Biophysical Properties and Functional Significance of Stem Water Storage Tissues in Neotropical Savanna Trees." *Plant, Cell & Environment* 30, no. 2: 236–248.

Scholz, F. G., N. G. Phillips, S. J. Bucci, F. C. Meinzer, and G. Goldstein. 2011. "Hydraulic Capacitance: Biophysics and Functional Significance of Internal Water Sources in Relation to Tree Size." In *Size-and Age-Related Changes in Tree Structure and Function*, 341–361. Cham: Springer Nature.

Stoffel, M. A., S. Nakagawa, and H. Schielzeth. 2021. "partR2: Partitioning R2 in Generalized Linear Mixed Models." *PeerJ* 9: e11414.

Tyree, M. T., and F. W. Ewers. 1991. "The Hydraulic Architecture of Trees and Other Woody Plants." *New Phytologist* 119, no. 3: 345–360.

Tyree, M. T., and S. Yang. 1990. "Water-Storage Capacity of Thuja, Tsuga and Acer Stems Measured By Dehydration Isotherms - The Contribution of Capillary Water and Cavitation." *Planta* 182: 420–426.

Tyree, M. T., and M. H. Zimmerman. 2013. *Xylem Structure and the Ascent of Sap*. Cham: Springer Science & Business Media.

Utsumi, Y., Y. Sano, S. Fujikawa, R. Funada, and J. Ohtani. 1998. "Visualization of Cavitated Vessels in Winter and Refilled Vessels in Spring in Diffuse-Porous Trees By Cryo-Scanning Electron Microscopy." *Plant Physiology* 117: 1463–1471.

Utsumi, Y., Y. Sano, J. Ohtani, and S. Fujikawa. 1996. "Seasonal Changes in the Distribution of Water in the Outer Growth Rings of *Fraxinus mandshurica var. japonica*: A Study By Cryo-Scanning Electron Microscopy." *IAWA Journal* 17: 113–124.

de Vries, S. M., M. Alan, and M. Bozzano, et al. 2015. "Pan-European Strategy for Genetic Conservation of Forest Trees and Establishment of a Core Network of Dynamic Conservation Units." In *European Forest Genetic Resources Programme (EUFORGEN)*, 40. Rome, Italy: Bioversity International.

Wolfe, B. T., and T. A. Kursar. 2015. "Diverse Patterns of Stored Water Use Among Saplings in Seasonally Dry Tropical Forests." *Oecologia* 179: 925–936.

Ziemińska, K., E. Rosa, S. M. Gleason, and N. M. Holbrook. 2020. "Wood Day Capacitance Is Related to Water Content, Wood Density, and Anatomy Across 30 Temperate Tree Species." *Plant, Cell & Environment* 43, no. 12: 3048–3067.

Supporting Information

Additional supporting information can be found online in the Supporting Information section.